Efficient semi-analytical method for the analysis of large finite connected slot arrays

van Katwijk, Alexander J.; Neto, Andrea; Toso, Giovanni; Cavallo, Daniele

DOI
10.1109/TAP.2022.3209272

Publication date
2022

Document Version
Final published version

Published in
IEEE Transactions on Antennas and Propagation

Efficient Semi-Analytical Method for the Analysis of Large Finite Connected Slot Arrays

Alexander J. van Katwijk, *Graduate Student Member, IEEE*, Andrea Neto, *Fellow, IEEE*, Giovanni Toso, *Senior Member, IEEE*, and Daniele Cavallo, *Senior Member, IEEE*

***Abstract*— We present an efficient method for the analysis of finite connected slot arrays in the presence of stratified media. The formulation is based on a spectral method of moments, where only one basis function is considered for each array element and one for each slot edge. An expression for the mutual impedance is derived in terms of a double spectral integral. Asymptotic extraction techniques are employed to largely reduce the computation time of one of the spectral integrals. For the other integral, when a guided wave contribution dominates the mutual coupling between two array elements, the result can be approximated as the residue of the spectral polar singularity, providing a closed-form solution of the coupling for elements at electrically large distances. The complete method enables simulations of entire finite arrays with hundreds or even thousands of elements in minutes. The same structure would require impractical computation time when analyzed with general-purpose commercial software. The method allows estimating the performance of finite connected arrays. This is particularly relevant because wideband connected arrays are known to exhibit higher edge effects compared to narrowband arrays, due to the high interelement mutual coupling.**

***Index Terms*— Antenna arrays, finite array simulations, finite edge effects, wideband arrays.**

I. Introduction

WIDEBAND wide-scanning phased arrays have become a favorable solution not only for multifunction radars [1], [2], but recently also for wireless and satellite communication applications [3], [4]. When limited space is available on complex platforms, an ultrawideband antenna array combining several functions in a shared aperture is often the desired option. Such an array is typically also required to scan the beam electronically over a large field of view while maintaining good matching and radiation performance. The state-of-the-art solutions for wideband wide-scanning phased arrays are based on tapered slot arrays [5], [6], [7], tightly coupled dipole arrays [8], [9], [10], and connected slot arrays [11], [12]. These three families of arrays have been demonstrated to achieve multioctave bandwidths with conical scan volumes larger than $\pm 45°$.

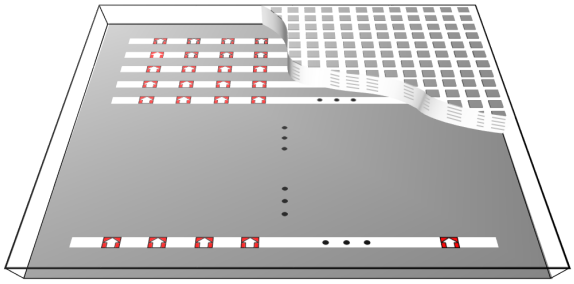

Fig. 1. Finite connected slot array with artificial dielectric superstrate.

Connected slot arrays are particularly advantageous among the different existing wideband array concepts because of their low-profile and planar architecture, which can be manufactured on a single multilayer printed circuit board at microwave frequencies. A connected slot array is an array of long slots fed at periodic locations to implement a wideband radiating aperture. Several designs based on connected slots are presented in [11], [12], [13], [14], and [15]. An effective approach to enhance the performance of the array in the presence of a backing reflector is proposed in [12] and consists of loading the array with artificial dielectric layers (ADLs). This array structure is shown in Fig. 1, which depicts the connected slot array and an artificial dielectric superstrate. The ADLs are layers of periodic subwavelength patches that can be designed such that they implement a wideband transformer to match the array impedance to free space without supporting surface waves.

Besides the planarity, another important advantage of connected arrays is that, unlike other ultrawideband arrays, they can be described with analytical expressions. The active input impedance of the elements can be written in closed form as a function of the geometrical parameters, as described in [16], [17], and [18]. The analytical model enables computation of the array unit cell main performance parameters within very little computation time, allowing the design of an array using a fast optimization procedure. However, the periodic unit cell approximation does not always represent the performance in

Manuscript received 23 March 2022; revised 15 June 2022; accepted 24 July 2022. Date of publication 30 September 2022; date of current version 19 January 2023. This work was supported in part by the European Space Agency (ESA) for the Project "Antenna User Terminal with Wide Angle Impedance Matching Metamaterial Radome" under Contract 4000127381/19/NL/AF. *(Corresponding author: Alexander J. van Katwijk.)*

Alexander J. van Katwijk, Andrea Neto, and Daniele Cavallo are with the Terahertz Sensing Group, Delft University of Technology, 2628 CD Delft, The Netherlands (e-mail: a.j.vankatwijk@tudelft.nl; a.neto@tudelft.nl; d.cavallo@tudelft.nl).

Giovanni Toso is with the Radio Frequency Payloads and Technology Division, European Space Research and Technology Centre (ESTEC), European Space Agency (ESA), 2200 AG Noordwijk, The Netherlands (e-mail: giovanni.toso@esa.int).

Color versions of one or more figures in this article are available at https://doi.org/10.1109/TAP.2022.3209272.

Digital Object Identifier 10.1109/TAP.2022.3209272

finite wideband arrays. Edge effects can be significant, and the active impedance of the individual elements can be considerably different from the infinite array approximation. This is especially true in connected arrays because the interelement connection allows guided waves generated at the edges to propagate along the array surface, affecting the impedance behavior of large portions of the array [22], [23], [24].

For this reason, numerical methods for the analysis of finite arrays [19], [20], [21] are needed to evaluate the variation of the output impedance seen by the transmit/receive modules connected to the antenna elements. Numerical methods specific for connected arrays are introduced in [23] and [25], but they are limited to finite-by-infinite arrays, which are assumed to be finite only in the H-plane and still periodic in the E-plane.

An attempt to include the finiteness in the E-plane was reported in [26]. However, this method used a discrete space Fourier transform to account for the finiteness of the slots, which assumed the spectral current in each slot to be the same except for a phase shift. This approximation was accurate enough in [26], because a high permittivity lens was considered above the array, reducing the mutual coupling between parallel slots. In more general stratifications, the current spectra cannot be assumed equal on the slots.

In this work, we introduce a semianalytical method for the analysis of finite-by-finite connected slot arrays, which does not rely on the approximation of equal current spectra on the slots. The method can be used for generic stratified media, so it can, for example, be combined with the known spectral Green's function of artificial dielectrics [27], [28] to simulate an entire array structure such as the one depicted in Fig. 1. Different acceleration techniques are implemented to speed up the computation of the coupling integrals. As a consequence, large arrays with hundreds or even thousands of elements can be analyzed with moderate computational resources. The complete method enables simulations of entire finite arrays using orders of magnitude less computational resources than commercial software. The finite array current distribution and all the relevant parameters, such as active impedances and radiation patterns, can be estimated using this method for generic complex excitation of the array elements.

II. Analysis Method

We consider an array of connected slots, as depicted in Fig. 2. The array consists of M parallel x-oriented slots, with indexes $m \in \{1, \ldots, M\}$ and centered at periodic locations $y = m\,d_y$. Each slot is fed by delta-gap generators at N locations spaced by d_x and is interrupted by metal terminations. The method assumes that the metal terminations are of a finite length such that the spectral solution for infinite slots can be used as in [25]. The array plane can be embedded within a general stratified medium along z that can, for instance, include dielectric substrates or superstrates, a backing reflector, or ADLs.

A. Space Domain Integral Equation

Following the procedure described in [26], an integral equation can be set up by imposing the continuity of the

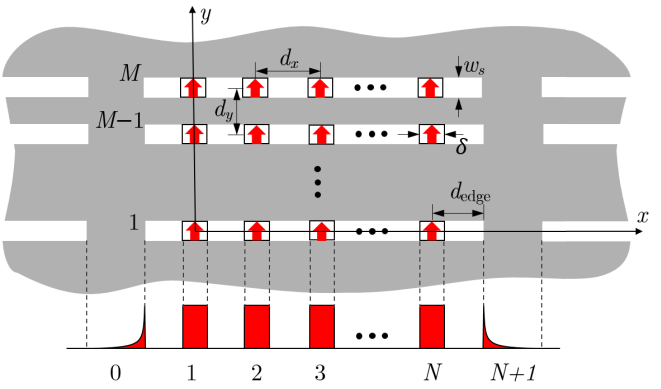

Fig. 2. Finite connected slot array with geometrical parameters and x-dependent basis functions on the feeding gaps and slot terminations, on each slot axis.

x-component of the magnetic field across the slots:

$$\iint m_x(x', y')\, g_{xx}(x - x', m d_y - y')\, dx'dy' = -j_{y,\text{gaps}}(x, m d_y) \tag{1}$$

where the left-hand side represents the magnetic field scattered by all the slots and observed on the axis of the mth slot ($y = m\,d_y$). The scattered field is written as a convolution between the equivalent magnetic current density on the slots (m_x) and the xx-component of the dyadic spectral Green's function (g_{xx}), relating the magnetic field to magnetic currents and accounting for the stratified medium above and below the slots. The right-hand side of (1) represents the sum of all surface electric currents flowing in the feeding gaps and the metal terminations

$$j_{y,\text{gaps}}(x, m d_y) = \sum_{n'=0}^{N+1} (i_{n'm} - Y_L v_{n'm})\, f_{n'}(x - x_{n'}) \tag{2}$$

where we assume the currents to be written as basis functions $f_{n'}$, defined on the feeds and terminations and centered at $x_{n'}$, multiplied by unknown coefficients. The basis functions are chosen as constant on the feeding gaps and edge singular on the metal terminations (see Fig. 2) and they are defined in closed form as in [25], both in space and spectral domains. The assumption of a single basis function per feed is accurate enough under the condition that the delta gaps are small compared to the wavelength, such that the current and voltage can be averaged on each gap. This choice of basis functions is not valid for the general shape of the slots, but specific for uniform slot width and rectangular delta-gap feeds.

The weights of the basis functions depend on the impressed currents $i_{n'm}$, the unknown average voltages in the gaps $v_{n'm}$, and the load admittance Y_L, according to the Norton equivalent circuit of the feeding ports as in Fig. 3. The impressed currents $i_{n'm}$ are imposed to be 0 for the passive metal terminations, that is, $i_{0\,m} = i_{N+1\,m} = 0$.

To solve the integral equation, we assume that the magnetic current is a separable-variable function on each slot

$$m_x(x', y') = \sum_{m'=1}^{M} v_{m'}(x')\, m_t(y' - m' d_y) \tag{3}$$

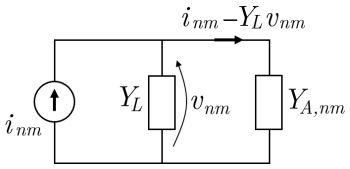

Fig. 3. Norton equivalent circuit of the feeding port of the array with indexes nm. $Y_{A,mn}$ is the active input admittance for the active port with indexes nm.

where $v_{m'}$ are unknown voltage distributions on the slots, while $m_t(y) = 2/(w_s\pi) \times (1-(2y/w_s)^2)^{-1/2}$ is an edge singular transverse distribution. The assumption that the magnetic current is variable separable and only oriented along x is valid under the condition that the slot width is uniform and narrow with respect to the wavelength. By replacing (3) and (2) in (1) and defining the function

$$d_{mm'}(x-x') = \int_{m'd_y-\frac{w_s}{2}}^{m'd_y+\frac{w_s}{2}} g_{xx}(x-x', md_y-y')m_t(y'-m'd_y)dy'. \tag{4}$$

One can simplify the integral equation as follows:

$$\sum_{m'=1}^{M}\int_{-\infty}^{\infty} d_{mm'}(x-x')v_{m'}(x')dx' = \sum_{n'=0}^{N+1}(Y_L v_{n'm} - i_{n'm}) f_{n'}(x-x_{n'}). \tag{5}$$

The function in (4) can be interpreted as the connected-array Green's function, associated with the field radiated by slot m' onto slot m. The introduction of this function enables the description of the magnetic current on the slots using only a limited number of basis functions located on the feeds and terminations. A more standard spectral domain approach would require discretization of the entire slot domain resulting in a large number of basis functions and heavy computation requirements.

B. Spectral Domain Integral Equation and Solution

Equation (5) can be written in the spectral domain as

$$\sum_{m'=1}^{M} D_{mm'}(k_x)V_{m'}(k_x) = \sum_{n'=0}^{N+1}(Y_L v_{n'm} - i_{n'm})F_{n'}(k_x)e^{jk_x x_{n'}} \tag{6}$$

where $V_{m'}(k_x)$ is the spectrum of the unknown voltage along the axis of each slot, k_x is the spectral counterpart of the spatial variable x, and $F_{n'}$ is the Fourier transform of the basis function $f_{n'}$. $D_{mm'}$ is the spectral version of (4) and is given by the k_y-spectral integral

$$D_{mm'}(k_x) = \frac{1}{2\pi}\int_{-\infty}^{\infty} G_{xx}(k_x,k_y)J_0\left(\frac{w_s k_y}{2}\right)e^{-jk_y(y_m-y_{m'})}dk_y \tag{7}$$

where J_0 is the zeroth-order Bessel function, representing the Fourier transform of the edge singular distribution across the slot, and G_{xx} is the xx-component of the dyadic spectral Green's function. The Green's function can be found as $G_{xx}(k_x,k_y) = (-i_{TE}k_x^2 + i_{TM}k_y^2)/(k_x^2+k_y^2)$, where i_{TE} and i_{TM} are the current solutions of the equivalent transmission lines representing the layered medium for TE and TM modes, respectively. The equivalent transmission lines for the ADL stratification were derived in [28].

When considering observation on the axes of all slots, (6) can be compactly written in matrix form as

$$\mathbf{D}(k_x)\mathbf{V}(k_x) = \sum_{n'=0}^{N+1}(Y_L\mathbf{v}_{n'} - \mathbf{i}_{n'})F_{n'}(k_x)e^{jk_x x_{n'}} \tag{8}$$

where $\mathbf{D}(k_x)$ is an M by M matrix consisting of the elements $D_{mm'}(k_x)$, $\mathbf{V}(k_x) = \{V_1(k_x),\ldots,V_M(k_x)\}$, $\mathbf{i}_{n'} = \{i_{n'1},\ldots,i_{n'M}\}$, and $\mathbf{v}_{n'} = \{v_{n'1},\ldots,v_{n'M}\}$. Inverting the D matrix leads to an expression for the voltage spectra as

$$\mathbf{V}(k_x) = \sum_{n'=0}^{N+1}\mathbf{D}^{-1}(k_x)(Y_L\mathbf{v}_{n'} - \mathbf{i}_{n'})F_{n'}(k_x)e^{jk_x x_{n'}}. \tag{9}$$

Projecting both LHS and RHS onto the nth test function (chosen as equal to the basis function, according to the Galerkin projection method) allows us to define a mutual impedance

$$Z_{nn'mm'} = -\frac{1}{2\pi}\int_{-\infty}^{\infty}\left(D^{-1}(k_x)\right)_{mm'}F_{n'}(k_x)F_n(-k_x) \times e^{-jk_x(x_n-x_{n'})}dk_x. \tag{10}$$

The mutual impedances in (10) fill the impedance matrix $\mathbf{Z}$, with which the unknown voltage vector can be found as

$$\mathbf{v} = (\mathbf{Z}_L + \mathbf{Z})^{-1}\mathbf{Z}_L\mathbf{Z}\mathbf{i} \tag{11}$$

where $\mathbf{v}$ and $\mathbf{i}$ are $(N+2) \times M$-element vectors describing the unknown voltages and the impressed currents at all basis functions. $\mathbf{Z}_L$ is a diagonal matrix containing the load impedance at each basis function, equal to $1/Y_L$ for the active feeds and 0 for the metal terminations. The currents flowing into each port are then given by $\mathbf{i}_A = \mathbf{Z}^{-1}\mathbf{v}$ and the active impedance at each of the feeds can be found as

$$Z_{A,nm} = \frac{v_{nm}}{i_{A,nm}}. \tag{12}$$

III. Analysis of the Spectral Integrals

The numerical method introduced in the previous section requires the computation of the spectral integrals in k_y and k_x, given by (7) and (10), respectively. These spectral integrals can be further studied to reduce computation time and highlight the different contributions.

A. Acceleration by Extraction of Asymptotic Part

For large values of k_y, the spectral Green's function is dominated by the reactive field surrounding the slot. For complex stratification such as the ADL in Fig. 4(a), the Green's function tends asymptotically to the Green's function G_{xx}^{∞} associated with a set of two homogeneous semiinfinite half-spaces as in Fig. 4(b). The media in these half-spaces

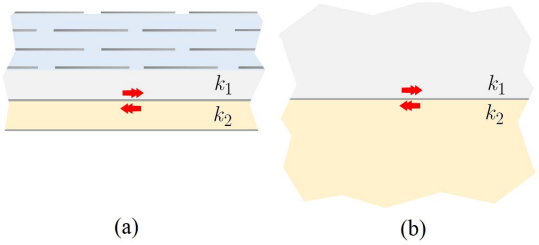

Fig. 4. (a) Initial stratification with ADL and backing reflector to define the stratified media Green's function for the problems above and below the slots. (b) Semiinfinite media to define the asymptotic Green's function for the upper and lower problems.

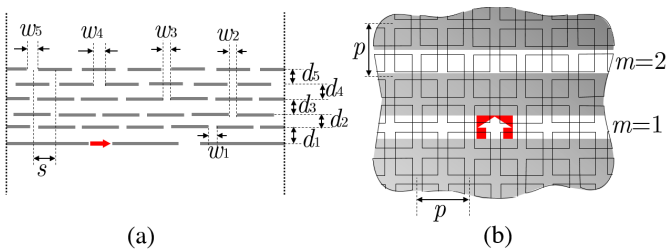

Fig. 5. (a) Side view and (b) top view of the ADL geometry considered, with two slots ($d_y = 0.19\lambda$, $w_s = 0.06\lambda$, where λ is the wavelength at the calculation frequency) and five-layer ADL ($p = 0.173\lambda$, $w_1 = w_2 = w_3 = 0.013\lambda$, $w_4 = w_5 = 0.022\lambda$, $d_1 = 0.009\lambda$, $d_2 = d_3 = 0.017\lambda$, $d_4 = 0.035\lambda$, $d_5 = 0.052\lambda$, $s = 0.5p$).

are taken as the closest media above and below the slot, with wavenumbers k_1 and k_2, respectively.

By subtracting and adding the homogeneous semiinfinite Green's function, (7) can be written as the sum of two integrals

$$\begin{aligned} D_{mm'}(k_x) &= \frac{1}{2\pi}\int_{-\infty}^{\infty}\left(I_{mm'}(k_x,k_y) - I^{\infty}_{mm'}(k_x,k_y)\right)dk_y \\ &\quad + \frac{1}{2\pi}\int_{-\infty}^{\infty} I^{\infty}_{mm'}(k_x,k_y))dk_y \\ &= D^{\text{diff}}_{mm'}(k_x) + D^{\infty}_{mm'}(k_x) \end{aligned} \tag{13}$$

with

$$I_{mm'}(k_x,k_y) = G_{xx}(k_x,k_y)J_0\left(\frac{w_s k_y}{2}\right)e^{-jk_y(y_m - y_{m'})} \tag{14}$$

$$I^{\infty}_{mm'}(k_x,k_y) = G^{\infty}_{xx}(k_x,k_y)J_0\left(\frac{w_s k_y}{2}\right)e^{-jk_y(y_m - y_{m'})}. \tag{15}$$

The first integral in (13) ($D^{\text{diff}}_{mm'}$) converges faster than the original integral ($D_{mm'}$) and can be evaluated over a reduced integration domain. The second integral ($D^{\infty}_{mm'}$) represents the spectral Green's function of slot pairs located at the interface between two semi-infinite homogeneous half-spaces and can be evaluated in closed form as [16]

$$\begin{aligned} D^{\infty}_{mm'}(k_x) &\approx \frac{-1}{2k_0\zeta_0}\sum_{i=1}^{2}\kappa_i^2 \\ &\quad \times \begin{cases} J_0\left(\frac{w_s}{4}\kappa_i\right)H_0^{(2)}\left(\frac{w_s}{4}\kappa_i\right), & \text{for } m = m' \\ H_0^{(2)}((y_{m'} - y_m)\kappa_i), & \text{for } m \neq m' \end{cases} \end{aligned} \tag{16}$$

where $\kappa_i = (k_i^2 - k_x^2)^{1/2}$, the subscripts $i = \{1, 2\}$ represent the upper and lower half-spaces, respectively, $H_0^{(2)}$ is the Hankel function of zeroth order and the second kind, and k_0 and ζ_0 are the free-space wavenumber and impedance.

An example is shown for the five-layer ADL shown in Fig. 5. The metal patches of the ADL are assumed to be in free space, and the media above and below the slot are also free space ($k_1 = k_2 = k_0$). The integrand as a function of the spectral variable k_y is shown in Fig. 6 for both the real stratification and the semi-infinite media. It can be seen that the difference between the two integrands becomes very small for $k_y > 10k_0$. This is confirmed by the relative error in Fig. 6(c) and (d), defined as $|I_{mm'} - I^{\infty}_{mm'}|/|I_{mm'}|$, which is below 1% for $k_y > 10k_0$.

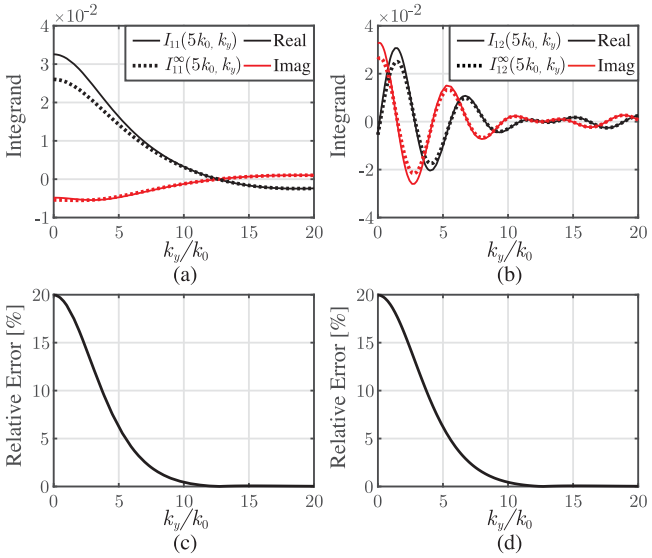

Fig. 6. Integrand as a function of k_y for $k_x = 5k_0$. Comparison between total integrand and semi-infinite dielectric case for (a) $m = m' = 1$ and (b) $m = 1 \neq m' = 2$. Relative error between total integrand and semi-infinite dielectric case for (c) $m = m' = 1$ and (d) $m = 1 \neq m' = 2$.

TABLE I
TIME RELATED TO THE CALCULATION OF $D^{-1}(k_x)$ IN (10) WITHOUT AND WITH USE OF THE ASYMPTOTIC EXTRACTION DESCRIBED IN (13)

	Without Acceleration	With Acceleration
5 slots	3 min, 14 sec	40 sec
20 slots	79 min, 23 sec	8 min, 39 sec

Extraction of the asymptotic part can be used to accelerate the integral in (7). The calculation time related to the matrix $\mathbf{D}^{-1}(k_x)$ is shown in Table I to be significantly reduced for arrays of 5 or 20 slots under the ADL in Fig. 5.

B. Residue Contribution

The integrand of the k_x-integral in (10) is characterized by a number of polar and branch singularities that represent guided and radiated waves, respectively. The nature and the number of poles are related to the specific dielectric stratification above and below the slot array. When the polar singularities are located on the real axis in the k_x-complex plane, they represent guided waves with no attenuation and are the dominant

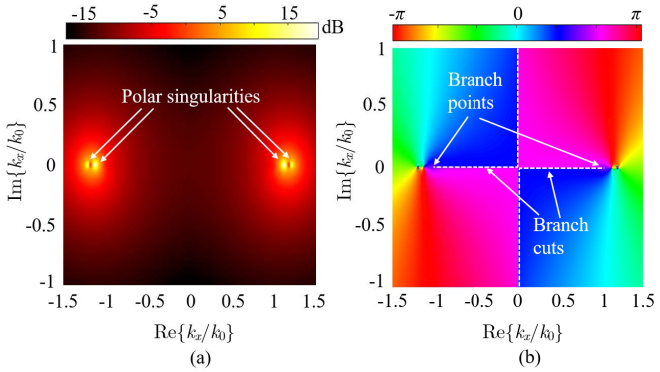

Fig. 7. Integrand of (10) in the k_x-complex plane for the stratification shown in Fig. 5. (a) Amplitude in dB and (b) phase of $(D^{-1}(k_x))_{12}$.

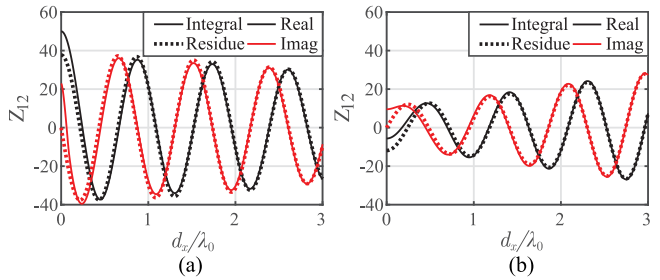

Fig. 8. Comparison between the complete integral and the residual contributions of the two poles is shown as a function of the distance between the two basis functions in the (a) same slot and (b) different slots.

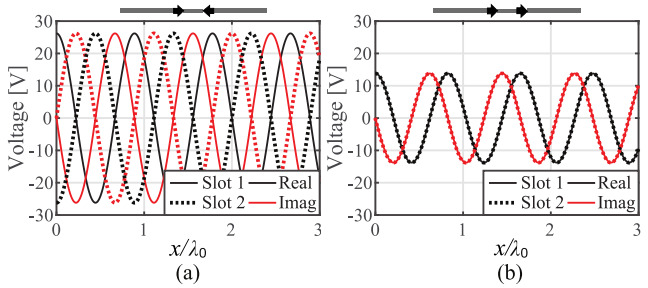

Fig. 9. Voltage distribution along a set of two slots, considering only (a) first polar contribution and (b) second polar contribution.

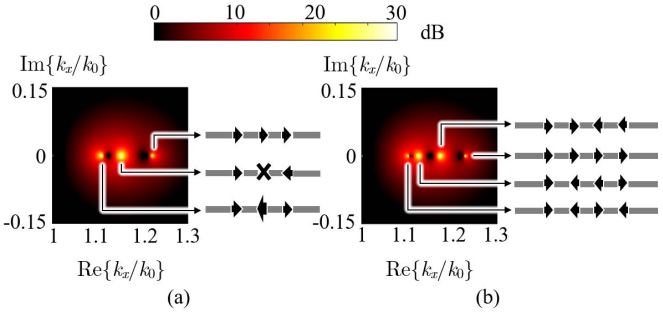

Fig. 10. Amplitude of $(D^{-1}(k_x))_{11}$ in the k_x-complex plane: location of the polar singularities for (a) three and (b) four slots under the ADL structure as in Fig. 5. Each pole represents a quasi-TEM mode supported by the ensemble of the slots.

contribution to the mutual impedance between basis functions at electrically large distances. As such, the mutual impedance between such elements can be approximated using the poles' residual contributions. This analytical approximation replaces the numerical computation of the integral, thus greatly simplifying the evaluation of the mutual impedances.

Assuming that the function $D_{mm'}$ has L poles indicated as $k_{xp1}, k_{xp2}, \ldots, k_{xpL}$, the residue contribution of the integral in (10) can be written as

$$Z_{nn'mm'} \approx \sum_{l=1}^{L} \frac{j F_{n'}(k_{xpl}) F_n(-k_{xpl}) e^{-jk_{xpl}(x_n - x_{n'})}}{\left.\frac{d(D^{-1}(k_x))_{mm'}}{dk_x}\right|_{k_x = k_{xpl}}}. \quad (17)$$

As an example, a 2×2 array is considered under the stratification shown in Fig. 5, and the function $(D^{-1}(k_x))_{12}$ is shown in the k_x-complex plane in Fig. 7. The polar and branch singularities are highlighted in the figure. A comparison between the complete integral and the residual contributions of the two poles is shown in Fig. 8 as a function of the distance between the two basis functions on the slot. The comparison is shown for basis functions in [Fig. 8(a)] the same slot and [Fig. 8(b)] different slots. For both cases, it can be seen that the mutual impedance is well approximated by the residue contribution for distances above a quarter wavelength.

C. Physical Meaning of Poles

A physical interpretation can be given to the polar singularities. Each pole can be associated with a guided mode supported by the combination of the various slots. To highlight this aspect, the voltage distribution along the slots is calculated on a set of two slots when only one feed is present on each slot. The voltage is calculated as the inverse Fourier transform of (9) and is equal to

$$v_m(x) = \frac{1}{2\pi} \int_{-\infty}^{\infty} V_m(k_x) e^{-jk_x x} dk_x. \quad (18)$$

The total voltage is computed using the residue theorem and the contribution from each of the two poles is plotted separately in Fig. 9. The voltage distributions on the two slots due to each pole are either equal or opposite, so the two poles correspond to the common and differential modes supported by the pair of slots.

While the closed-form solution of the integral as in (17) avoids the numerical computation of the coupling integrals, it must be noted that the number of poles is proportional to the number of slots composing the array. This aspect is illustrated in Fig. 10 where the position of the poles is shown in the complex plane for three and four slots. Each pole represents a quasi-transverse electromagnetic (TEM) mode supported by the slots. This is in line with the expectation that $N_c - 1$ TEM modes are supported by a transmission line with N_c conductors. Therefore, for large arrays, the search of the poles can become more complex than the original numerical integration and may thus no longer be convenient. Moreover, when a large number of poles occur in the range $k_0 < k_x < 1.3\ k_0$, it can become difficult to distinguish them and isolate the individual contributions.

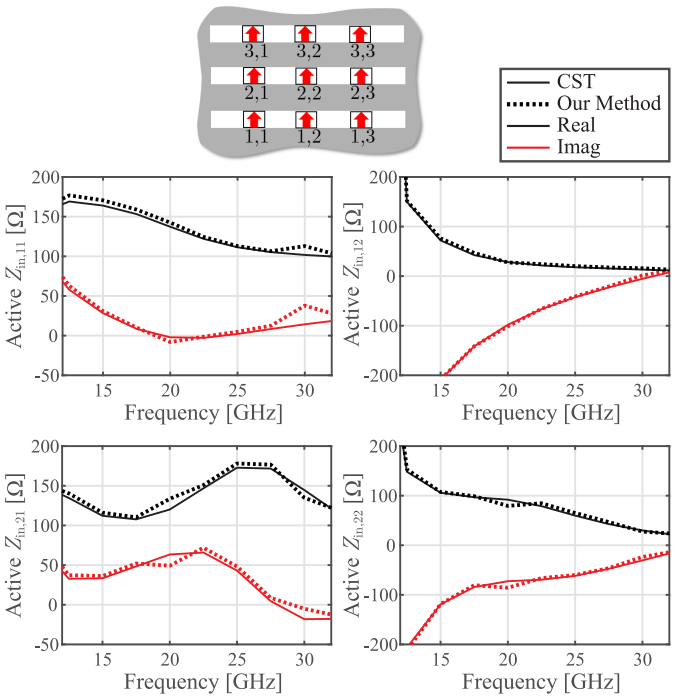

Fig. 11. Comparison between CST and MoM of the active input impedance of each element of a 3 × 3 array in free space, with $d_x = d_y = 0.45\lambda$, $w_s = 0.05\lambda$, $\delta = 0.05\lambda$, $d_{edge} = 0.25\lambda$, and $Z_L = 100\ \Omega$, where λ is the wavelength at 31 GHz.

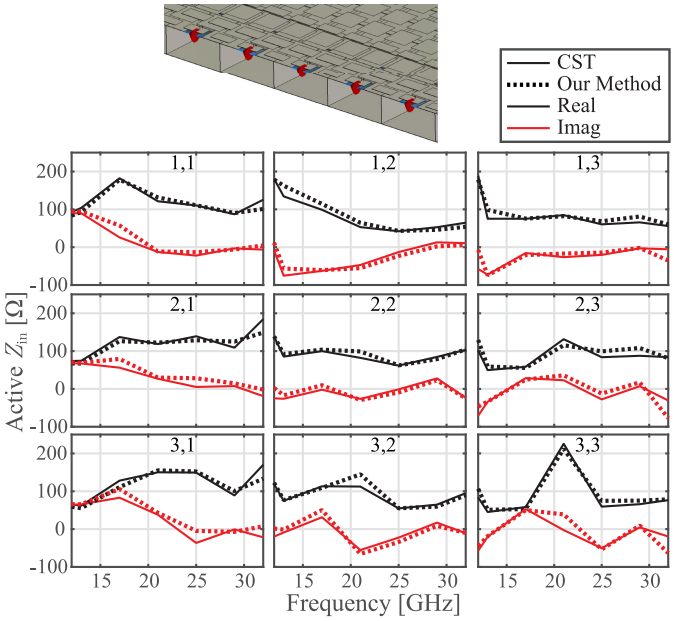

Fig. 12. Comparison between CST and MoM of the active input impedance of each element of a 5 × 5 array with a backing reflector and a five-layer ADL superstrate. Vertical walls are included below the slot plane. The geometrical parameters are $d_x = d_y = 4.35$ mm, $w_s = 1.4$ mm, $\delta = 2$ mm, $d_{edge} = 2.4$ mm, distance from backing reflector $h = 1.9$ mm, relative permittivity of the substrate $\varepsilon_r = 2.2$. The ADL is in free-space with $p = d_x/2$, $w_1 = 0.64$ mm, $w_2 = w_3 = 0.32$ mm, $w_4 = w_5 = 0.5$ mm, $d_1 = 0.23$ mm, $d_2 = d_3 = 0.45$ mm, $d_4 = 0.83$ mm, $d_5 = 1.2$ mm, and $s = 0.5p$.

IV. Validation

A. Impedance

The method is validated using the commercial solver CST Studio Suite. First, a 3 × 3 array is considered in free-space, with $d_x = d_y = 0.45\lambda$, $w_s = 0.05\lambda$, $\delta = 0.05\lambda$, $d_{edge} = 0.25\lambda$, and $Z_L = 100\ \Omega$. The active input impedance of the elements for broadside scanning is presented in Fig. 11, showing a very good agreement between our model and CST. Only four elements of the array are shown, since all the others are included by symmetry.

A 5 × 5 finite array with a backing reflector and loaded by a 5-layer artificial dielectric is simulated in CST and using our method. Vertical walls are considered between parallel slots as in [12]. Fig. 12 shows a good agreement between the results given by CST and those generated by our method. For this example, the computation time was 2 min for seven frequency points with our method, versus 2 h in CST.

B. Radiation Patterns

The radiation patterns can also be computed from the voltage spectrum in (9) by using the stationary phase point method. The generic component of the radiated magnetic field can be expressed as

$$H_{\{x,y,z\}}(\theta_o, \phi_o, r) \approx jk_{zo} G_{\{x,y,z\}x}(k_{xo}, k_{yo}) M(k_{xo}, k_{yo}) \frac{e^{-jk_0 r}}{2\pi r} \tag{19}$$

where (θ_o, ϕ_o, r) refer to an observation point in the far-field and $k_{xo} = k_0 \sin\theta_o \cos\phi_o$, $k_{yo} = k_0 \sin\theta_o \sin\phi_o$, and $k_{zo} = k_0 \cos\theta_o$. The 2-D magnetic current spectrum on the array aperture is

$$M(k_x, k_y) = \sum_{m=1}^{M} V_m(k_x) J_0(k_y w/2) e^{jk_y m d_y}. \tag{20}$$

For example, for the 3 × 3 array in free space considered in the previous section, the H-plane embedded patterns of the corner and central elements are shown as red dotted curves

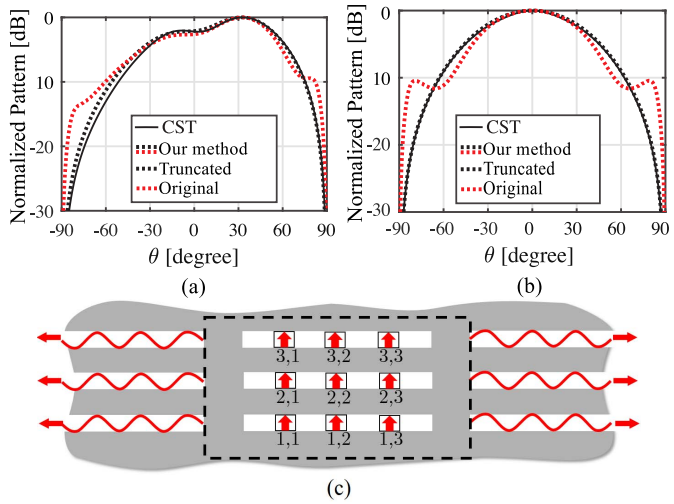

Fig. 13. 3 × 3 connected slot array in free space. H-plane embedded patterns of (a) corner (1, 1) and (b) central (2, 2) elements, with and without windowing of the aperture field. (c) Finite length metal terminations at the slot edges with fictitious waves propagating in the slots outside the array. A rectangular window (dashed rectangle) is used to exclude these waves from the results.

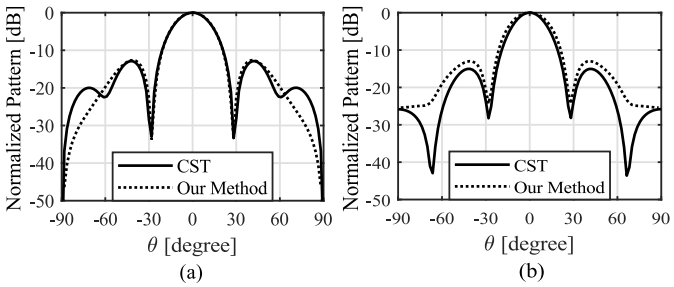

Fig. 14. Radiation patterns for the 5 × 5 array with ADL as the one considered in Fig. 12. (a) H-plane $\phi = 0°$. (b) E-plane $\phi = 90°$.

in Fig. 13(a) and (b). It can be seen that a discrepancy with CST occurs at large angles close to 90°. This discrepancy arises due to the assumption of finite length metal terminations at the slot edges, which is used to simplify the procedure by exploiting the spectral solutions of the infinite slot. The extension of the slots after this finite termination enables the propagation of fictitious residual waves along the infinite slots outside the array [see Fig. 13(c)]. This effect can be removed from the results by replacing the total spectrum V_m with a truncated version $V_{m,\text{trunc}}$ that includes only the array aperture [dashed rectangle in Fig. 13(c)] and cuts out the aperture field in the passive slots outside the array. This can be obtained mathematically by applying the inverse Fourier transform ($\mathcal{F}^{-1}\{\cdot\}$) of (9), multiplying by a rectangular window $\text{rect}_{\text{array}}(x)$ including only the finite slot region and re-applying the Fourier transform ($\mathcal{F}\{\cdot\}$)

$$V_{m,\text{trunc}}(k_x) = \mathcal{F}\{\mathcal{F}^{-1}\{V_m(k_x)\}\text{rect}_{\text{array}}(x)\}. \tag{21}$$

The patterns after truncation are also shown in Fig. 13(a) and (b), and they are closer to the CST solutions.

The patterns in the presence of the ADL can also be calculated since the spectral Green's function of ADLs is known. For the same 5 × 5 array with ADL considered in Fig. 12, the patterns on the two main planes are shown in Fig. 14.

V. Large Array Performance

A. Impedance Matching

To show the capabilities of the method, a large array is simulated containing 32 × 32 elements. The array is based on the same unit cell as in Fig. 12. Our method is used to analyze the effects of the finiteness on such an array. The resulting active VSWR of each element is shown in Fig. 15(a)–(c) for various scanning conditions. It is seen that, while most elements are close to the infinite array approximation, some deviate from it quite significantly. This information is relevant in array design to estimate the amount of power that is reflected in the output of the power amplifiers feeding the individual elements. On the other hand, the total matching efficiency of the array, determined from the total input and reflected power as $(P_{\text{in}} - P_{\text{reflected}})/P_{\text{in}}$, is shown in Fig. 15(d) to be within a few percent of the infinite array.

To determine the position of the elements that exhibit a higher VSWR, colormaps of the VSWR for each element

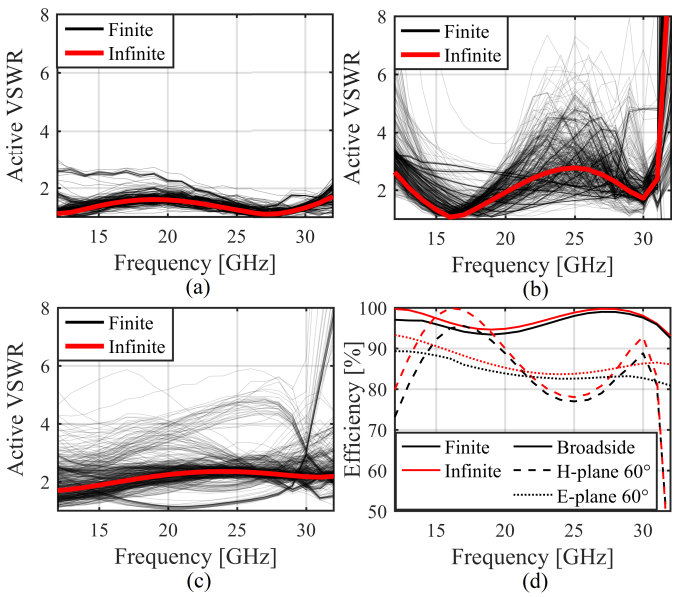

Fig. 15. Active VSWR for each element in a 32 × 32 connected slot array when scanning to (a) broadside, (b) 60° on the H-plane, and (c) 60° on the E-plane. (d) Resulting in matching efficiency.

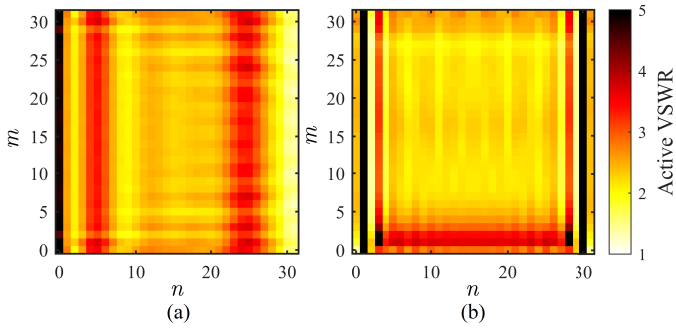

Fig. 16. Maps of the active VSWR of the elements across the array for scanning to 60° at 31 GHz in the (a) H-plane and (b) E-plane.

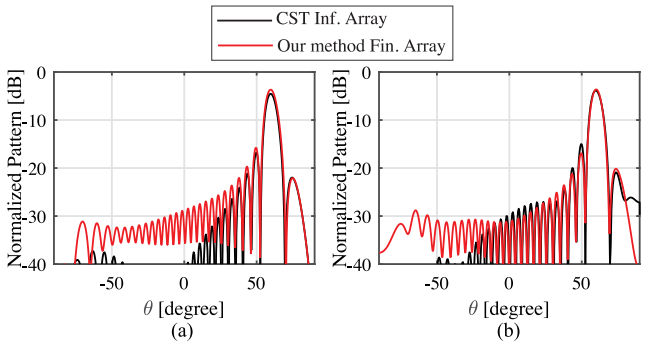

Fig. 17. Radiation patterns at 30 GHz of a 32 × 32 finite array based on the unit cell shown in 12 scanning to 60° on (a) H-plane and (b) E-plane. The patterns are normalized to the maximum at the broadside.

(n, m) are shown in Fig. 16 for different frequencies and scanning conditions. It is seen that the greatest mismatch is seen at the edges of the array and that the majority of elements have a VSWR lower than 3.

B. Radiation Patterns

The proposed spectral method also provides the radiation patterns of the finite array. The standard approach for estimating the pattern of finite arrays is the windowing technique [29], [30], which simply multiplies the unit cell active element pattern by the array factor. However, this technique does not account for the variations of the impedance across the array. The radiation patterns of the finite array for scanning to 60° in the two main planes are shown in Fig. 17, where they are compared to the windowing approximation. It is evident that for large arrays, the two methods provide a similar estimation of the patterns with differences primarily in the sidelobes.

VI. Conclusion

We presented a numerical method to analyze planar-connected arrays with ADLs. The method is based on a spectral domain approach with a limited number of basis functions, equal to $(N + 2) \times M$, for an array of $N \times M$ elements. The mutual impedance is efficiently evaluated by extraction of asymptotic parts and residue contributions of the polar singularities.

The method was validated using CST and enables finite array simulations with large numbers of elements to estimate the effects of the finiteness on the active impedance and the radiation patterns.

References

[1] C. Renard and M. Soiron, "Wideband multifunction airborne antennas," in *Proc. Int. Radar Conf. Surveill. Safer World*, Bordeaux, France, Oct. 2009, pp. 1–3.

[2] S. Kemkemian and M. Nouvel-Fiani, "Toward common radar & EW multifunction active arrays," in *Proc. IEEE Int. Symp. Phased Array Syst. Tech.*, Oct. 2010, pp. 777–784.

[3] M. H. Novak, F. A. Miranda, and J. L. Volakis, "Ultra-wideband phased array for millimeter-wave ISM and 5G bands, realized in PCB," *IEEE Trans. Antennas Propag.*, vol. 66, no. 12, pp. 6930–6938, Dec. 2018.

[4] A. J. V. Katwijk, A. Neto, G. Toso, and D. Cavallo, "Design of wideband wide-scanning dual-polarized phased array covering simultaneously both the Ku- and the Ka-satcom bands," in *Proc. 14th Eur. Conf. Antennas Propag. (EuCAP)*, Mar. 2020, pp. 1–3.

[5] J. J. Lee, S. Livingston, and R. Koenig, "A low-profile wide-band (5:1) dual-pol array," *IEEE Antennas Wireless Propag. Lett.*, vol. 2, pp. 46–49, 2003.

[6] W. Elsallal *et al.*, "Charateristics of decade-bandwidth, balanced antipodal Vivaldi antenna (BAVA) phased arrays with time-delay beamformer systems," in *Proc. IEEE Int. Symp. Phased Array Syst., Technol.*, Waltham, MA, USA, Oct. 2013, pp. 111–116.

[7] J. T. Logan, R. W. Kindt, and M. N. Vouvakis, "A 1.2–12 GHz sliced notch antenna array," *IEEE Trans. Antennas Propag.*, vol. 66, no. 4, pp. 1818–1826, Apr. 2018.

[8] J. P. Doane, K. Sertel, and J. L. Volakis, "A wideband, wide scanning tightly coupled dipole array with integrated balun (TCDA-IB)," *IEEE Trans. Antennas Propag.*, vol. 61, no. 9, pp. 4538–4548, Sep. 2013.

[9] J. A. Kasemodel, C. C. Chen, and J. L. Volakis, "Wideband planar array with integrated feed and matching network for wide-angle scanning," *IEEE Trans. Antennas Propag.*, vol. 61, no. 9, pp. 4528–4537, Sep. 2011.

[10] S. S. Holland, D. H. Schaubert, and M. N. Vouvakis, "A 7–21 GHz dual-polarized planar ultrawideband modular antenna (PUMA) array," *IEEE Trans. Antennas Propag.*, vol. 60, no. 10, pp. 4589–4600, Oct. 2012.

[11] J. J. Lee, S. Livingston, R. Koenig, D. Nagata, and L. L. Lai, "Compact light weight UHF arrays using long slot apertures," *IEEE Trans. Antennas Propag.*, vol. 54, no. 7, pp. 2009–2015, Jul. 2006.

[12] W. H. Syed, D. Cavallo, H. T. Shivamurthy, and A. Neto, "Wideband, wide-scan planar array of connected slots loaded with artificial dielectric superstrates," *IEEE Trans. Antennas Propag.*, vol. 64, no. 2, pp. 543–553, Feb. 2016.

[13] D. Cavallo, W. H. Syed, and A. Neto, "Connected-slot array with artificial dielectrics: A 6 to 15 GHz dual-Pol wide-scan prototype," *IEEE Trans. Antennas Propag.*, vol. 66, no. 6, pp. 3201–3206, Jun. 2018.

[14] Y. Li, S. Xiao, and B.-Z. Wang, "A wideband circularly polarized connected parallel slot array in the presence of a backing reflector," *IEEE Access*, vol. 8, pp. 26517–26523, 2020.

[15] Y. Li, S. Xiao, C.-H. Hu, and Z. Yao, "A low-profile light-weight wideband connected parallel slot array for wide-angle scanning," *IEEE Trans. Antennas Propag.*, vol. 68, no. 2, pp. 813–823, Feb. 2020.

[16] A. Neto and S. Maci, "Green's function for an infinite slot printed between two homogeneous dielectrics. Part I: Magnetic currents," *IEEE Trans. Antennas Propag.*, vol. 51, no. 7, pp. 1572–1581, Jul. 2003.

[17] A. Neto and J. J. Lee, "Ultrawide-band properties of long slot arrays," *IEEE Trans. Antennas Propag.*, vol. 54, no. 2, pp. 534–543, Feb. 2006.

[18] D. Cavallo, A. Neto, and G. Gerini, "Analytical description and design of printed dipole arrays for wideband wide-scan applications," *IEEE Trans. Antennas Propag.*, vol. 60, no. 12, pp. 6027–6031, Dec. 2012.

[19] P. De Vita, A. Freni, F. Vipiana, P. Pirinoli, and G. Vecchi, "Fast analysis of large finite arrays with a combined multiresolution—SM/AIM approach," *IEEE Trans. Antennas Propag.*, vol. 54, no. 12, pp. 3827–3832, Dec. 2006.

[20] D. J. Ludick, R. Maaskant, D. B. Davidson, U. Jakobus, R. Mittra, and D. de Villiers, "Efficient analysis of large aperiodic antenna arrays using the domain Green's function method," *IEEE Trans. Antennas Propag.*, vol. 62, no. 4, pp. 1579–1588, Apr. 2014.

[21] H. Bui-Van *et al.*, "Fast and accurate simulation technique for large irregular arrays," *IEEE Trans. Antennas Propag.*, vol. 66, no. 4, pp. 1805–1817, Apr. 2018.

[22] O. A. Civi and P. H. Pathak, "Array guided surface waves on a finite planar array of dipoles with or without a grounded substrate," *IEEE Trans. Antennas Propag.*, vol. 54, no. 8, pp. 2244–2252, Aug. 2006.

[23] A. Neto, D. Cavallo, and G. Gerini, "Edge-born waves in connected arrays: A finite × infinite analytical representation," *IEEE Trans. Antennas Propag.*, vol. 59, no. 10, pp. 3646–3657, Oct. 2011.

[24] D. Cavallo, W. H. Syed, and A. Neto, "Equivalent transmission line models for the analysis of edge effects in finite connected and tightly coupled arrays," *IEEE Trans. Antennas Propag.*, vol. 65, no. 4, pp. 1788–1796, Apr. 2017.

[25] R. M. van Schelven, D. Cavallo, and A. Neto, "Equivalent circuit models of finite slot antennas," *IEEE Trans. Antennas Propag.*, vol. 67, no. 7, pp. 4367–4376, Jul. 2019.

[26] D. Cavallo and A. Neto, "A connected array of slots supporting broadband leaky waves," *IEEE Trans. Antennas Propag.*, vol. 61, no. 4, pp. 1986–1994, Apr. 2013.

[27] D. Cavallo and C. Felita, "Analytical formulas for artificial dielectrics with nonaligned layers," *IEEE Trans. Antennas Propag.*, vol. 65, no. 10, pp. 5303–5311, Oct. 2017.

[28] D. Cavallo and R. M. van Schelven, "Closed-form analysis of artificial dielectric layers with non-periodic characteristics," in *Proc. 13th Eur. Conf. Antennas Propag.*, Krakow, Poland, Apr. 2019, pp. 1–5.

[29] A. Ishimaru, R. Coe, G. Miller, and W. Geren, "Finite periodic structure approach to large scanning array problems," *IEEE Trans. Antennas Propag.*, vol. AP-33, no. 11, pp. 1213–1220, Nov. 1985.

[30] A. K. Skrivervik and J. R. Mosig, "Analysis of finite phase arrays of microstrip patches," *IEEE Trans. Antennas Propag.*, vol. 41, no. 8, pp. 1105–1114, Aug. 1993.

Alexander J. van Katwijk (Graduate Student Member, IEEE) received the B.Sc. and M.Sc. *(cum laude)* degrees in electrical engineering from the Delft University of Technology (TU Delft), Delft, The Netherlands, in 2017 and 2019, respectively, where he is currently pursuing the Ph.D. degree with the Terahertz Sensing Group.

In TU Delft, he works on analytical/numerical techniques in electromagnetics, cross-polarization reduction techniques, and wideband connected arrays.

Andrea Neto (Fellow, IEEE) received the Laurea degree *(summa cum laude)* in electronic engineering from the University of Florence, Florence, Italy, in 1994, and the Ph.D. degree in electromagnetics from the University of Siena, Siena, Italy, in 2000.

Part of his Ph.D. degree was developed at the European Space Agency Research and Technology Centre, Noordwijk, The Netherlands. He was with the Antenna Section, European Space Agency Research and Technology Centre, for over two years. From 2000 to 2001, he was a Post-Doctoral Researcher with the California Institute of Technology, Pasadena, CA, USA, where he was with the Submillimeter Wave Advanced Technology Group. From 2002 to 2010, he was a Senior Antenna Scientist with The Netherlands Organization for Applied Scientific Research Defense, Security, and Safety, The Hague, The Netherlands. In 2010, he became a Full Professor of applied electromagnetism with the Department of Microelectronics, Delft University of Technology, Delft, The Netherlands, where he formed and currently leads the THz Sensing Group. His research interests include the analysis and design of antennas with an emphasis on arrays, dielectric lens antennas, wideband antennas, EBG structures, and THz antennas.

Dr. Neto is a member of the Technical Board of the European School of Antennas and the Steering Committee of the Network of Excellence NEWFOCUS, dedicated to focusing on techniques in mm- and submillimeter-wave regimes. He is also an organizer of the course on antenna imaging techniques. He was a recipient of the European Research Council Starting Grant to perform research on advanced antenna architectures for THz sensing systems in 2011, the H. A. Wheeler Award for the Best Applications Paper in the IEEE TRANSACTIONS ON ANTENNAS AND PROPAGATION in 2008, the Best Innovative Paper Prize of the European Space Agency Antenna Workshop in 2008, and the Best Antenna Theory Paper Prize of the European Conference on Antennas and Propagation (EuCAP) in 2010. He served as an Associate Editor for the IEEE TRANSACTIONS ON ANTENNAS AND PROPAGATION from 2008 to 2013 and the IEEE ANTENNAS AND WIRELESS PROPAGATION LETTERS from 2005 to 2013.

Giovanni Toso (Senior Member, IEEE) received the Laurea *(cum laude)* and Ph.D. degrees and the Post-Doctoral Fellowship from the University of Florence, Florence, Italy, in 1992, 1995, and 1999, respectively.

In 1996, he was the Visiting Scientist of the Laboratoire d'Optique Electromagnétique, Marseille, France. In 1999, he was the Visiting Scientist of the University of California (UCLA) at Los Angeles, Los Angeles, CA, USA, he received the Scholarship from Alenia Spazio, Rome, Italy. He has been appointed as a Researcher with the Radio Astronomy Observatory of the Italian National Council of Researches (CNR), Rome, Italy. Since 2000, he has been with the Antenna and Submillimeter Waves Section, European Space Research and Technology Centre (ESTEC), European Space Agency (ESA), Noordwijk, The Netherlands. He has been initiating and contributing to several research and development activities on satellite antennas based on arrays, reflectarrays, discrete lenses, and reflectors. In particular, in the field of onboard satellite antennas, he has been coordinating activities on multibeam antennas (active and passive) mainly for telecom applications. In the field of terminal antennas for telecom applications, he has been initiating several research and development activities on reconfigurable antennas with electronic, mechanical, and hybrid scanning; some of these antennas are now available as commercial products. He has been initiating and supporting the development of the commercial software tool QUPES by TICRA, now used worldwide, for the analysis and design of periodic and quasi-periodic surfaces, such as reflectarrays, frequency selective surfaces, transmitarrays, and polarizers. He has been coauthoring the Best Paper at the 30th ESA Antenna Workshop and the Most Innovative Paper at the 30th and 36th ESA Antenna Workshops. He holds more than 20 international patents.

Dr. Toso was a Co-Editor of the Special Issue on Active Antennas for Satellite Applications in the *International Journal of Antennas and Propagation* in 2009. In 2014, he was a Guest Editor of the Special Issue on Innovative Phased Array Antennas Based on Non-Regular Lattices and Overlapped Subarrays published in the IEEE TRANSACTIONS ON ANTENNAS AND PROPAGATION, where he was an Associate Editor from 2013 to 2016. Since 2010, together with Dr. P. Angeletti, he has been instructing short courses on multibeam antennas and beamforming networks during international conferences [IEEE APS, IEEE International Microwave Symposium (IMS), the IEEE International Conference on Wireless Information Technology and Systems (ICWITS), European Conference on Antennas and Propagation (EuCAP), and European Microwave Week (EuMW)] that have been attended by more than 800 participants. In 2018, he has been the Chairperson of the 39th ESA Antenna Workshop on "Multibeam and Reconfigurable Antennas" and received, together with Prof. A. Skrivervik, the Best Teacher Award of the European School of Antennas (ESoA) out of 101 teachers. He is the organizer of the new ESoA course on active antennas.

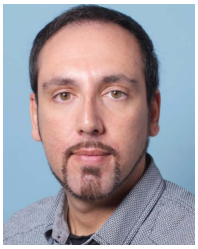

Daniele Cavallo (Senior Member, IEEE) received the M.Sc. degree *(summa cum laude)* in telecommunication engineering from the University of Sannio, Benevento, Italy, in 2007, and the Ph.D. degree *(cum laude)* in electromagnetics from the Eindhoven University of Technology, Eindhoven, The Netherlands, in 2011.

From 2007 to 2011, he was with the Antenna Group, The Netherlands Organization for Applied Scientific Research, The Hague, The Netherlands. From 2012 to 2015, he was a Post-Doctoral Researcher with the Microelectronics Department, Delft University of Technology (TU Delft), Delft, The Netherlands. In 2015, he joined the Chalmers University of Technology, Gothenburg, Sweden, as a Visiting Researcher. He is currently an Associate Professor with the Terahertz Sensing Group, TU Delft. He has authored or coauthored more than 150 papers published in peer-reviewed international journals and conference proceedings. His current research interests include analytical and numerical methods for antenna characterization, the design of antenna arrays, and on-chip antennas.

Dr. Cavallo is a member of the European Association on Antennas and Propagation (EurAAP), a Co-Coordinator of the EurAAP working group "Active Array Antennas," and Management Committee Member of the COST Action "future communications with higher-symmetric engineered artificial materials (SyMat)." He was a recipient of the Best Innovative Paper Prize at the European Space Agency Antenna Workshop in 2008, the Best Paper Award in Electromagnetics and Antenna Theory at the 11th European Conference on Antennas and Propagation (EuCAP) in 2017, and the 250 keuro "Veni" Personal Grant from The Netherlands Organization for Scientific Research (NW0) in 2015. His students received the Best Student Paper Award at EuCAP 2013, the Special Mention at EuCAP 2015, the Else Kooi Prize in 2016, and the Honorable Mention at the IEEE Antennas and Propagation Society International Symposium in 2019. He is also an Associate Editor of the IEEE TRANSACTIONS ON ANTENNAS AND PROPAGATION.